Part II
Environmental Impacts of LIP Emplacement

3

Global Warming and Mass Extinctions Associated With Large Igneous Province Volcanism

David P. G. Bond[1] and Yadong Sun[2]

ABSTRACT

The coincidence of large igneous province (LIP) eruptions with at least three, if not all, of the Big Five biotic crises of the Phanerozoic implies that volcanism is a key driver of mass extinctions. Many LIP-induced extinction scenarios invoke global warming, caused primarily (but not exclusively) by greenhouse gases emitted at the site of LIP emplacement and by contact metamorphism of carbon-rich host rocks. Here we explore (1) the climate-changing products of volcanism including sulfur dioxide (SO_2), carbon dioxide (CO_2) and methane (CH_4) from eruptions, contact metamorphism, and melting (dissociation) of gas hydrates; (2) their deadly effects, including marine anoxia and thermal stress; (3) increasingly sophisticated paleotemperature proxies (e.g., $\delta^{18}O$ of shell material) through case studies of the best-known LIP-warming-extinction nexi; and (4) global warming through the lens of the putative Anthropocene extinction.

3.1. INTRODUCTION

Large igneous province (LIP) eruptions coincided with at least three, if not all, of the Big Five mass extinctions of the Phanerozoic, as well as several lesser crises (Table 3.1). This temporal link implies that volcanism is a key driver of mass extinction. Most, but not all, mass extinctions (somewhat controversially) are associated with pulses of global warming as indicated by paleotemperature proxies such as the $\delta^{18}O$ record of marine fossils that preserve the signatures of the ancient oceans in which they lived. As is feared for the modern planet, global warming is linked to a range of synergistic stresses on land and in the oceans. These include marine anoxia, an oft-cited extinction mechanism in the oceans that features in many extinction scenarios (Table 3.1). Warming also causes thermal stress to organisms both on land and in the oceans where satisfying increased oxygen demands for a higher metabolism can be problematic. Several decades of research have revealed that there is no single, common driver of extinctions; it is clear that the effects of global warming did not act alone in past extinction scenarios. Instead, warming was likely part of a lethal cocktail of LIP effects that also include acidification, ozone depletion, toxic metal poisoning, and numerous others (examined in detail elsewhere in this volume; see also the reviews of Bond & Grasby, 2017, and Ernst & Youbi, 2017).

In this chapter, we focus on the climate-changing products of volcanism and the deadly conditions that these can induce. We provide an overview of the history of paleothermometry and the range of temperature proxies available to us today, and examine these through the lens of two of the greatest hothouses in Earth history: the Permian-Triassic and Paleocene-Eocene intervals. Finally, we consider how past episodes of warming provide context for modern, anthropogenic climate change.

[1] *Department of Geography, Geology and Environment University of Hull, Hull, United Kingdom*

[2] *GeoZentrum Nordbayern, Universität Erlangen-Nürnberg, Erlangen, Germany*

Large Igneous Provinces: A Driver of Global Environmental and Biotic Changes, Geophysical Monograph 255, First Edition.
Edited by Richard E. Ernst, Alexander J. Dickson, and Andrey Bekker.

DOI: 10.1002/9781119507444.ch3

Table 3.1 Phanerozoic Mass Extinctions Since the Early Cambrian, With Associated LIPs, Episodes of Climate Change, Marine Anoxia, and Carbon Cycle Perturbations

Extinction	Associated LIP	Climate change	Marine anoxia?	Carbon isotope shift
Botomian (Early/Middle Cambrian)	Kalkarindji	?	Yes	−4‰
Dresbachian (Cambrian)	None	Warming?	Yes	+5‰
End Ordovician	Speculated	Cooling (phase 1) and warming (phase 2)	Partly	+7‰ followed by −7‰
Ireviken Event (Silurian)	None	Cooling?	Yes	−4‰ imposed on a positive trend
Mulde Event (Silurian)	None	Cooling?	Yes	+4‰
Lau Event (Silurian)	None	Cooling?	Yes	+6‰
Kačák Event (Devonian)	None	Warming?	Yes	+2‰
Thaganic Event (Devonian)	None	Warming?	Yes	+2‰
Frasnian-Famennian (Devonian)	Viluy Traps, PDD?	Warming (+9°C) imposed on cooling pusles	Yes	Up to +4‰
Hangenberg Event (End Devonian)	PDD?	Warming and cooling (including glaciation)	Yes	Up to +6‰
Capitanian (Permian)	Emeishan Traps	? both have been invoked	Yes (only regionally)	−6‰ (in China)
End Permian	Siberian Traps	Warming (+15°C)	Yes	Up to −8‰
Smithian/Spathian (Triassic)	Siberian Traps (late stages)	Warming (+6°C)	Yes	−6‰ followed by +6‰
Carnian (Triassic)	Wrangellia	Warming (+7°C)	Yes	−5‰
End Triassic	CAMP	Warming (+6°C)	?	−5‰
Early Jurassic	Karoo/Ferrar	Warming (+7°C)	Yes	−7‰ in $\delta^{13}C_{org}$ −3‰ in $\delta^{13}C_{carb}$
End Cretaceous	Deccan Traps	Warming (+4°C)	No	−2‰

Note: The Big Five extinction events are highlighted in bold text. PDD = Pripyat-Dnieper-Donets rift system; CAMP = Central Atlantic Magmatic Province. Modified from Bond and Grasby (2017).

3.2. LARGE IGNEOUS PROVINCES AND CLIMATE CHANGE

3.2.1. Short-Term Cooling

It might seem odd to begin this chapter with a section on cooling, but this is probably the most tangible climatic effect of volcanism because it operates on human timescales. Thus, major episodes of historical volcanism have caused significant environmental damage and global cooling over timescales of months to years (e.g., Briffa et al., 1998). The Mount Pinatubo eruption of 1991 was followed by a fall in global temperature of ~0.5°C for 3 years. The substantially larger 1783–1784 fissure eruptions at Laki were followed by extreme cooling of 5°C in Iceland (Wood, 1992) and the eastern United States recorded its coldest ever winter in 1783–1784 (Scarth, 2001). Basaltic lavas, such as those associated with Laki, can carry large amounts, up to 1.5 wt%, of sulfur (Jugo et al., 2005), which degasses as sulfur dioxide (SO_2) at low pressure. Laki injected approximately 122 Mt of SO_2 into the upper troposphere / lower stratosphere (Thordarson & Self, 1993, 2003), where its rapid dispersal and atmospheric conversion to sunlight-blocking sulfate aerosols was a key driver of cooling (e.g., Robock, 2000). The cooling effects of SO_2 can last for 2–3 years after an eruption, but rarely longer, because SO_2 reacts with water in the atmosphere to form H_2SO_4 that is efficiently removed as acid rain, itself implicated in major terrestrial mass extinctions (Black et al., 2014; Sephton et al., 2015). The observed effects of major historical volcanism cannot simply be scaled up for LIP scenarios. Sulfate aerosol formation is limited by the amount of water vapor in the atmosphere (Pinto et al., 1989), which in turn limits the cooling effect (e.g., Schmidt et al., 2012). Schmidt et al. (2016) used a global aerosol model to estimate the effects of individual, decade-long Deccan Traps eruptions (ca. 66 Mya) and estimated that a single pulse would result in a global surface temperature fall of 4.5°C followed by a 50 year recovery period. Thus, LIP-scale eruptions could in theory cause more prolonged cooling than smaller eruptions, but only if they were frequent, of high volume, and sustained for several centuries at a time. However, the modeling of Schmidt et al. (2012, 2016) has shown that although the duration of cooling might scale up with larger eruptions, the intensity of cooling does not. Despite recent advances in the radio-isotopic dating of LIPs and paleothermometry techniques, the geological record is not sufficiently resolved to test whether sustained, LIP-induced cooling has happened during a mass extinction. The brief duration of volcanogenic cooling events has long been recognized (e.g., Sear et al., 1987; Rampino et al., 1988) and Schmidt et al.'s study (2016) serves to remind us that such events are unlikely to be recorded even in high-resolution deep-time paleothermometry where achieving decadal-centennial sampling is extremely difficult.

3.2.2. Long-Term Warming

Other than SO_2, water vapor (H_2O) and carbon dioxide (CO_2) are volumetrically the most important volcanic gases. Water vapor acts as a positive radiative forcing agent in the stratosphere that counteracts the cooling effects of sulfate aerosols, but like SO_2, its effects are short lived. Carbon dioxide, on the other hand, is a well-known greenhouse gas with effects lasting for millennia, a major concern for the modern planet in which the rate of atmospheric CO_2 is increasing at rates faster than at any time since perhaps the Paleocene-Eocene (e.g., Bowen et al., 2015); even more worrying estimates put the modern rate of change at 10 times that of the Paleocene-Eocene (Foster et al., 2018). Thus, CO_2 remains in the atmosphere much longer than SO_2: a fifth of CO_2 is still there several thousands of years after it is injected (Archer, 2005).

Could LIP-derived CO_2 have driven global warming? Self et al. (2005) estimated that a single LIP flow of volume 10,000 km^3 (containing 0.5 wt.% CO_2 that fully degassed) would inject around 13 Gt of CO_2 into the atmosphere. Given the annual anthropogenic CO_2 flux to the atmosphere is around 37 Gt (about 10 Gt carbon; IPCC, 2014), a single, isolated eruption of this scale is unlikely to have been an agent of great change. However, a diagnostic feature of LIPs is their enormous volumes: Bryan and Ernst (2008) defined LIPs as having volumes $>0.1 \times 10^6$ km^3, 75% of which was emplaced in ~1–5 Myr. If 75% of the smallest possible LIP (by definition) was emplaced over 5 Myr, that would require 7.5 flows of the volume used in Self et al.'s (2005) calculations to occur, on average, every 666,666 years. Hardly the stuff of mass extinctions, considering the entire LIP would inject around as much CO_2 in 5 million years that humans currently manage in just over two and a half years! The likelihood, however, is that the LIPs associated with mass extinctions are significantly more voluminous, and were probably emplaced rather more quickly (<< 1 Myr). Thus, the cumulative effects of repeated, closely spaced flood basalt eruptions could potentially induce global warming as the longer residence time of CO_2 offsets the shorter-term cooling effects of SO_2. The temporal resolution of mass extinction records is not detailed enough to evaluate this with certainty.

3.2.3. Missing Links

The simple calculations above imply shortcomings in the LIP-warming-extinction model, especially when one compares the numbers with those associated with modern

anthropogenic CO_2 emissions. Thus, the total CO_2 released by one of the largest continental LIPs of all time, the Siberian Traps, has been estimated to have been 30,000 Gt (Courtillot & Renne, 2003), 10 times the mass in today's atmosphere. At today's rate of anthropogenic emissions, it would take just 800 years to inject that mass of CO_2, and while some might forecast the end-Permian style global warming in the next 800 years, few would argue that the entire Siberian Traps were emplaced in such a short time. It has been noted that the volume of the Siberian Traps volcanics alone is insufficient to have generated global warming on the scale predicted, nor was it large enough to have provided the huge amounts of isotopically light carbon required to generate the associated ca. 5–6‰ negative carbon isotope shift (e.g., Berner, 2002; Payne & Kump, 2007). There must be a missing link.

One of the earliest models to address the apparent mismatch between the volume of some LIPs and their lethality (some of the largest LIPs had little impact on the extant fauna and flora) invokes the voluminous release of methane from gas hydrates. Today, there is concern that global warming could lead to extensive deposits of methane hydrates that are trapped (frozen) in the hydrate stability zone (Kvenvolden, 1993) to melt and escape to the atmosphere (Kennett et al., 2000). Methane is a potent greenhouse gas that would amplify the global warming effects of CO_2, in turn destabilizing more hydrates with further warming effects. This positive feedback loop, sometimes referred to as a "clathrate gun", might have created a runaway greenhouse rather quickly (Kennett et al., 2000, 2003) and has been implicated in global warming at the Permian-Triassic (Krull & Retallack, 2000; Krull et al., 2000), Triassic-Jurassic (Ruhl et al., 2011), and Paleocene-Eocene (Dickens, 1999; Dickens et al., 1997; Katz et al., 1999) boundaries. However, the potency of gas hydrates in driving warming is questionable because hydrate melting is a self-limiting endothermic reaction. In their model of the gas hydrate contribution to Late Permian global warming, Majorowicz et al. (2014) concluded that hydrate disassociation is not instantaneous process but occurs over 100 to 400 kyr intervals in any one location. Their model shows melting happens first in lower latitudes before progressing to higher latitudes as the climate warms, with hydrate release lasting as long as a million years (Majorowicz et al., 2014). During such long periods of time, methane would oxidize to the far less potent greenhouse gas, CO_2 (Cicerone & Oremland, 1988). Further, methane hydrates released in deep water would most likely be rapidly oxidized in the water column, greatly reducing, or completely negating, their climatic effects (Rupple, 2011).

In the past decade, other LIP-warming models have emerged. Sobolev et al. (2011) revised Courtillot and Renne's (2003) estimate of the Siberian Traps' CO_2 budget dramatically upward when they suggested that recycled ocean crust may form up to 15% of plumes, and this material would yield substantial amounts of CO_2 during partial melting. Driven off ahead of the ascending magma, an estimated 170,000 Gt (nearly 60 times the amount in today's atmosphere) of CO_2 may have been released in a few, closely spaced blasts, with devastating results. Sobolev et al.'s (2011) model has an order of magnitude more CO_2 than previous estimates being injected into the Permian atmosphere in a geological instant. This is a game-changer, but the goalposts had shifted several years earlier, when Svensen et al. (2004) suggested that the warming responsible for the Paleocene-Eocene Thermal Maximum was the result of thousands of Gt of methane released by organic-rich sediments being baked by high-level intrusives (a scenario refined by Frieling et al. (2016) and subsequently challenged by Gutjahr et al. (2017)). So-called thermogenic gases represent a potentially deadly additional source of methane and CO_2, and they also neatly account for major negative carbon isotope excursions associated with LIP eruptions because thermogenic gases will have the lighter isotopic signature of their source sedimentary organic matter. Svensen et al.'s (2004) theory soon found favor in the Permian-Triassic community with suggestions that significant CH_4 and CO_2 was generated by intrusions into coal (Grasby et al., 2011; Retallack & Krull, 2006; Retallack et al., 2006) and other organic rich sedimentary rocks (e.g., Deegan et al., 2016; Jones et al., 2016; Svensen et al., 2009). Svensen's and Sobolev's hypotheses changed the way we think about LIPs, and apparently (for now) provided the missing pieces to the LIP-warming-extinction jigsaw.

3.3. GLOBAL WARMING AS AN AGENT OF EXTINCTION

3.3.1. Direct Effects of Warming on the Biosphere

The most obvious direct effect of global warming on organisms is that of thermal stress. When the planet warms, the geographic range of a species usually expands poleward in response, often leading to oddities such as hippopotami and hyenas roaming the lead author's now rather cool home county of Yorkshire, England, as recently as the Ipswichian interglacial, just over 100 kyr ago (Harkness et al., 1976). But if an organism or population cannot migrate, could warming lead to species extinction? Warming increases aerobic metabolism in animals (Frederich & Pörtner, 2000; Pörtner, 2002) approximately scaled to the Q_{10} law (generally doubling with every 10°C increase; Cossins et al., 1987; Knoll et al., 2007). A higher metabolism requires more oxygen, and becomes impossible for animals to maintain when

their oxygen demand exceeds their aerobic scope (the oxygen-limited thermal tolerance model of Pörtner, 2010). Baseline metabolic rate might therefore be considered a key predictor of survivorship during extreme warming events: in theory, groups with sluggish metabolisms (e.g., brachiopods) should fare better than those with higher metabolisms (e.g., bivalves) because a doubling of each group's metabolism is of greater magnitude for the latter. However, bivalves experienced a well-below-average generic extinction magnitude of ~60% during the Permian-Triassic crisis (Tu et al., 2016) and also did relatively well during several other crises that are associated with warming. This might be because active organisms can elevate their metabolic rate during bursts of activity and so have higher aerobic scope than less active organisms (Pörtner, 2010). The role of warming and thermal stress in extinction scenarios is complicated by the fact that there are very few truly sessile organisms in the marine realm: most nonmotile groups have a planktonic larval stage ensuring good dispersal that allows the species to migrate into favorable settings. Numerous other factors influence response to warming, including preexposure, which dictates that the tolerance of an organism to extremes of temperature is different depending on where it lives (Russell et al., 2013).

At the base of the food chain, temperature also has a profound effect on primary production in both marine and terrestrial ecosystems, with implications for the nutrient balance of the planet from deep time to the present day. In theory, warming increases gross primary productivity, although numerous studies of recent extreme weather events (particularly droughts) have demonstrated the opposite relationship (e.g., Zhao & Running, 2010). Clearly, the net effects of warming on productivity and food web structure are complex (see Petchey et al., 1999, for an introduction to this topic). Warming has been shown to strengthen the role of consumers in the food web, ultimately leading to a reduction in the total biomass of the food web despite increases in primary productivity (O'Connor et al., 2009). The implication is that relatively minor changes in ocean temperature could drive major shifts in marine productivity and food web structure that could destabilize entire ecosystems. This is a major concern in future global warming scenarios, but it is unclear how these shifts have played out in the past.

3.3.2. Indirect Effects of Warming

Warming also indirectly damages ecosystems because it reduces the capacity of water to dissolve oxygen, and therefore promotes the development of marine anoxia, prolonged exposure to which causes death by asphyxia without selectivity (Diaz & Rosenberg, 1995). Anoxia is a proximal killer invoked in several mass extinction scenarios (Table 3.1), where it has left abundant facies and geochemical evidence (Bond & Grasby, 2017, and references therein). The expansion of oxygen minimum zones into shelf areas, critical components of marine ecosystems, and beyond, at the very time that warming increased demand for oxygen (see above), is a seemingly indiscriminate extinction driver, encapsulated by the death of ca. 1.5 million pilchards at Redondo Beach, California, during a minor, but inescapable anoxic event in 2011 (e.g., Stauffer et al., 2012). Perhaps in response, many animal groups have evolved specialists that tolerate and even thrive in oxygen-poor conditions. These specialists can decrease their oxygen consumption and scale up anaerobic metabolism as required (Pörtner & Grieshaber, 1993), such as during transient anoxic episodes, giving them a better chance of survival from such events, and, in theory, even thriving during mass extinctions caused by anoxia (Fig. 3.1).

Figure 3.1 A Griesbachian (earliest Triassic) bedding surface covered in valves of the opportunistic epifaunal bivalve *Claraia* (Langdai, western Guizhou, China). *Claraia* is considered a highly evolved specialist that can decrease its oxygen consumption during transient anoxic episodes, allowing it to proliferate in the Early Triassic. Such groups are much more likely to survive short-lived dysoxic-anoxic events, although no aerobic group can survive long periods of total anoxia, which is an indiscriminate killer implicated in several mass extinctions. Hammer for scale is 29cm long. Photograph by Paul Wignall, used with permission.

While anoxia is clearly a deadly consequence of warming, numerous other parts of the climate system are also affected during warming events, with less obvious implications. Thus, climate change influences hydrology, runoff to the oceans, nutrient supply, and upwelling intensity, all of which feature as agents of regional or global extinction in several scenarios. For example, the Late Devonian (Frasnian-Famennian) crisis (the second crisis of the Big Five) is associated with globally widespread anoxia

during the Upper Kellwasser Event (e.g., Bond et al., 2004). In their models, Algeo et al. (1995) and Algeo and Scheckler (1998) attribute the expansion of anoxia to the rise of land plants and terrestrialization of Earth, with enhanced pedogenesis increasing the supply of nutrients to the oceans, stimulating primary productivity and oxygen consumption like never before. This theory has recently found support in the Devonian osmium isotope record, which indicates that the Upper Kellwasser Event was associated with a major increase in riverine runoff (Percival et al., 2019). Further up the stratigraphic record, death-by-turbidity due to enhanced weathering and riverine runoff is implicated in the Permian-Triassic extinction (Algeo & Twitchett, 2010), and the slow recovery from that crisis might also be a function of indirect effects of warming. Thus, nitrogen isotope data from continental margin settings (i.e., upwelling zones) reveal a decline in N availability through the Early Triassic, which likely stressed primary production and contributed to a sluggish marine recovery (Grasby et al., 2016; Grasby et al., 2020; Sun et al., 2019).

In summary, the interactions between the direct and indirect effects of warming and their impacts on the biosphere are complex, but greater knowledge of these will inform our predictions of the ecological impact of the current phase of climate change. To understand how these interacted in deep time, we need reliable proxies for each of the factors associated with extinctions, and, in particular, for past temperatures.

3.4. PALEOTEMPERATURE PROXIES

Paleotemperature reconstruction has long been a fundamental aspiration for geoscientists. Ultimately, paleothermometry aims to provide quantitative measures of temperature fluctuations of air or seawater in the geological past, thereby allowing comparisons of local, regional, and global conditions in the ancient and modern. Several paleothermometry techniques have been established in recent decades: oxygen isotope ratios ($\delta^{18}O$) of shelly fossils; trace metal (e.g., Mg/Ca) ratios; biomarkers of certain long-chain lipids (e.g., TEX_{86} and alkenones); and most recently, clumped isotopes. Here, we provide a brief summary of the advantages and key caveats associated with each method, and point the interested reader in the direction of more thorough texts on these.

3.4.1. Oxygen Isotopes

Oxygen Isotope Fractionation

Oxygen has three naturally occurring stable isotopes: ^{16}O, ^{17}O, and ^{18}O with atmospheric abundances of 99.759%, 0.037%, and 0.204%, respectively. In oceanography and climate science, oxygen isotope ratios are most commonly expressed in δ notation and measured in per mille (‰) relative to a standard:

$$\delta^{18}O = \left[\left({}^{18}O/{}^{16}O \right)_{sample} / \left({}^{18}O/{}^{16}O \right)_{standard} - 1 \right] \times 1000\% \quad (3.1)$$

Isotopic fractionation is a process that changes the relative abundances of different isotopes of an element. Most fractionation of oxygen in natural environments is mass-dependent fractionation, that is, the partitioning of different isotopes is proportional to the differences in masses of those isotopes and involves physical processes and chemical reactions. The hydrocycle can cause large oxygen isotope fractionation because the water molecule (H_2O) has different masses: $^{1}H_2{}^{16}O$ is the lightest and $^{2}H_2{}^{18}O$ is the heaviest (^{3}H is radioactive and is excluded here). The light water molecule is prone to phase changes (e.g., vaporization or condensation) and can be transported farther than the heavy water molecule. The result is that ice, glacial water, and snowmelt generally have very low $\delta^{18}O$, precipitation at the poles can have a $\delta^{18}O$ composition as light as –60‰. In comparison, $\delta^{18}O$ of precipitation in equatorial regions is often much heavier. As light water is continuously vaporized and transported away, equatorial seawater is enriched in ^{18}O. If this is not balanced by an isotopically light freshwater input, the $\delta^{18}O$ composition of equatorial seawater can be as heavy as ~2‰. Spatial variations in evaporation and precipitation result from the dynamics of Earth's climate, but ultimately these lead to the heterogeneity of $\delta^{18}O$ in the global ocean (Fig. 3.2).

Because the isotopically lightest water is concentrated in snow and ice, the volume of the latter on the continents has a major impact on the mass balance of $\delta^{18}O$ of the entire hydrosphere. When large volumes of ice exist, the average global $\delta^{18}O$ of seawater is heavier. An ice-free world has seawater with a light $\delta^{18}O$ signal. Therefore, $\delta^{18}O$ of seawater actually reflects both regional evaporation and precipitation and global changes in continental ice volume.

Isotope fractionation during chemical reactions involves the breaking and forming of chemical bonds. The energy required for breaking a heavier bond is slightly higher than that required to break a lighter bond. This subtle difference leads to a predictable isotope fractionation, which is fundamental to $\delta^{18}O$ paleothermometry. Thus, when a shell is precipitated in an aquatic system, the $\delta^{18}O$ of the newly formed shell records the repartitioning of different O isotopes from the ambient water. This repartition, if occurring at isotopic equilibrium, is a function of the temperature and $\delta^{18}O$ of the ambient water. Similarly, the $\delta^{18}O$ of terrestrial organisms depends on air and body temperatures as well as the $\delta^{18}O$ of ingested water. Ingested water may have multiple sources, adding complications to terrestrial paleothermometry.

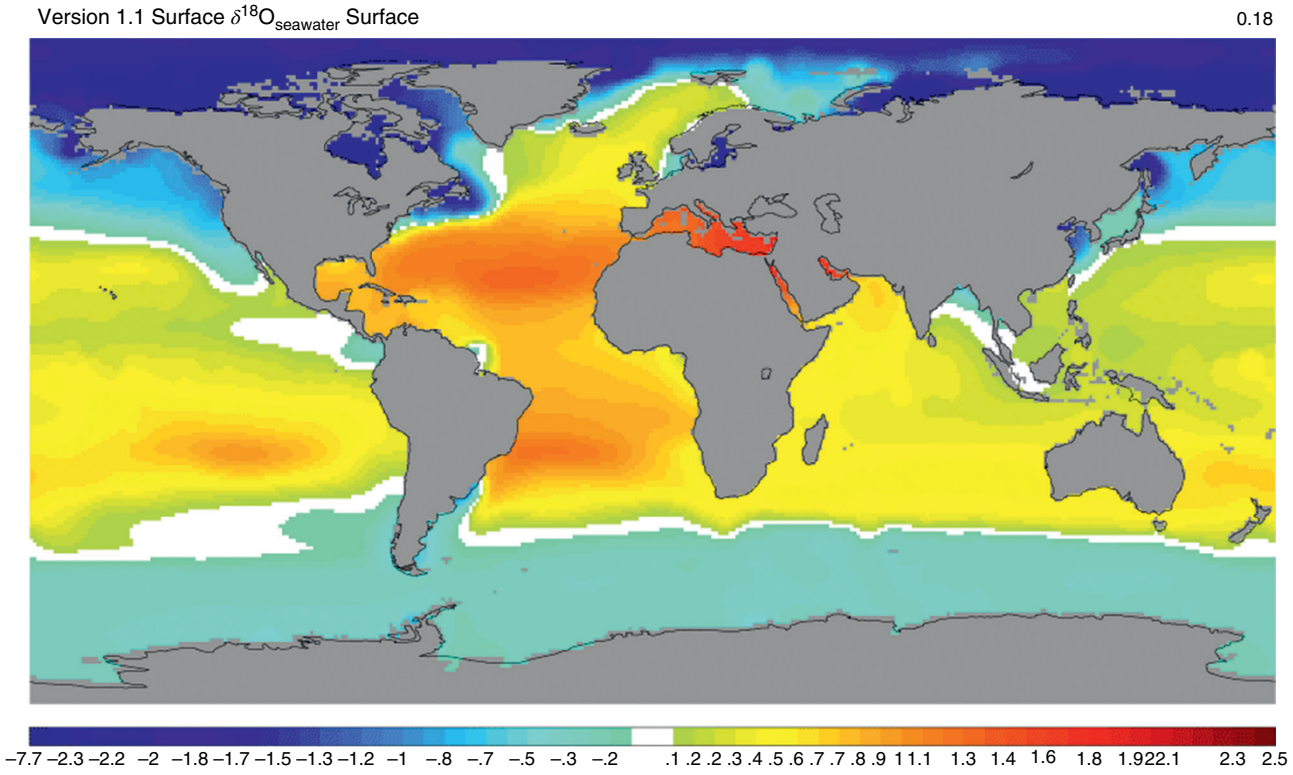

Figure 3.2 Oxygen isotope composition of global ocean, showing large heterogeneity and latitudinal changes in seawater $\delta^{18}O$. From Schmidt et al. (1999) and used with permission of the authors.

Deep-Time $\delta^{18}O$ Paleothermometry

Paleothermometry in deep time is difficult, more so with increasing age of studied material because of problems related to burial and solid-state diffusion of isotopes between fossils and host rocks. Suitable materials for $\delta^{18}O$ thermometry include ice cores, carbonate (e.g., brachiopod or foraminifer shells, or speleothems), biogenic phosphate (e.g., conodonts and fish teeth), and biogenic silica (e.g., diatoms). They must meet the following criteria: (1) precipitation of the material occurred at, or near, isotopic equilibrium; and (2) materials are not diagenetically altered. The first criterion renders several fossil groups that exhibit "vital effects" unsuitable (the vital effect is biologically mediated isotope fractionation out of equilibrium with ambient water, and it occurs in echinoderms, red algae, corals, some foraminifers, and coccolithophores). All sedimentary rocks are subject to diagenetic changes, but these do not necessarily alter the original isotopic signature. However, criterion (2) rules out most material that was originally composed of aragonite but has been altered to low magnesium calcite. Aragonite is metastable at surface temperature and pressure, and alteration to calcite occurs over tens to hundreds of Myr. Thus, only a few groups are suitable for paleothermometry. For Cretaceous and younger intervals, pelagic and benthic foraminifers are most commonly used, whereas studies of older intervals tend to use brachiopods, belemnites, or conodonts for $\delta^{18}O$ analyses (Fig. 3.3). Conodont apatite is now recognized as among the best materials for ancient paleothermometry. The abundance of conodonts in Cambrian to Triassic strata makes them useful index fossils, and they define many GSSPs (Global Stratotype Sections and Points) (Aldridge & Purnell, 1996; Knell, 2013). This also means that high-resolution temperature records can usually be achieved. It is important to note that because the conodont animal lived in the water column, the reconstructed temperatures are of seawater, rather than of the seafloor or the underlying sediments. The taxa chosen for study are those where the ranges of water depths inhabited are well constrained, and a calibration enables the calculated temperatures to be adjusted to sea-surface temperatures (or similar).

The key caveat associated with oxygen isotope paleothermometry, other than complications arising from diagenesis, is that the $\delta^{18}O$ of seawater in the geological past is unknown. Assuming $\delta^{18}O_{seawater}$ is a constant is a simple solution for most paleoenvironmental studies since major changes in global $\delta^{18}O_{seawater}$ in a short

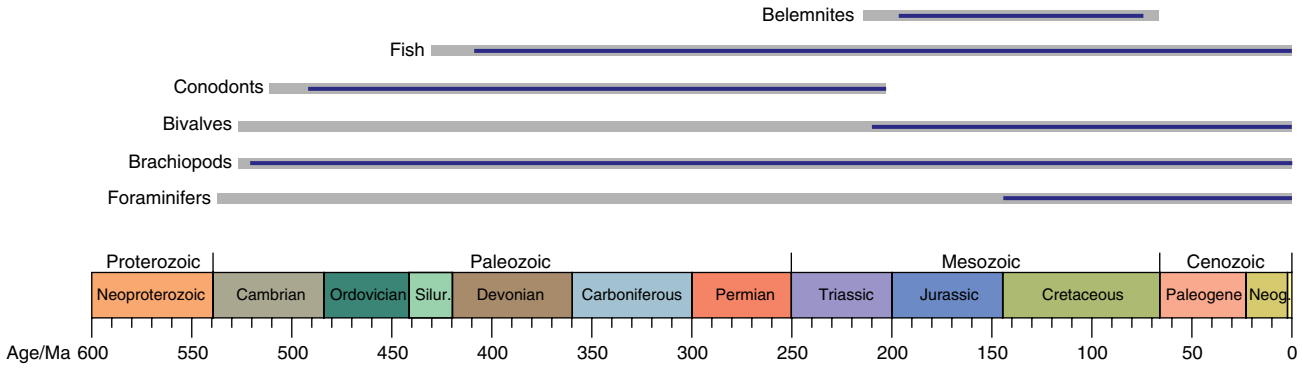

Figure 3.3 Fossil groups used for paleotemperature reconstruction in Cambrian to Recent studies. Gray lines = temporal range of group (bivalves, brachiopods, foraminifers, and fish are extant); blue lines = stratigraphic range in which each group has paleothermometry applications. The temporal range used here for fish does not include jawless fish, whose "teeth" are actually horny structures that have no application in oxygen isotope paleothermometry. Neog = Neogene. The yellow box at the far right of the timescale represents the Quaternary.

(i.e., <1 Myr) interval are unlikely. The $\delta^{18}O_{seawater}$ is often presumed to be -1‰ if the studied interval was an ice-free world, or between 0 and +2‰ for minor to global glacial intervals. Given that $\delta^{18}O_{seawater}$ can be assumed constant in most studies (unless the study interval is very long), the absolute value of $\delta^{18}O_{seawater}$ used only affects the temperature calibration; the magnitude of calculated temperature changes is unaffected. However, $\delta^{18}O_{seawater}$ is almost certainly not constant during glacial-interglacial transitions due to the ice volume effect. Paleothermometry of waxing and waning ice ages is a particular challenge. An additional complication is that assuming a $\delta^{18}O_{seawater}$ of -1‰ for an ice-free world provides some unlikely results for pre-Devonian times. Calculated paleotemperatures often exceed 50°C and can be up to 70°C (Veizer et al., 1999). These are unrealistically high and incompatible with oceans that were clearly hospitable to varied life. Such data have prompted intense debate over whether there have been secular changes in $\delta^{18}O_{seawater}$ throughout the Phanerozoic. It has been suggested that $\delta^{18}O_{seawater}$ has evolved over time and has become ~6‰ heavier since the Cambrian (Veizer & Prokoph, 2015) or ~13‰ heavier since ~3.4 Ga (Jaffrés et al., 2007). This trend toward heavy $\delta^{18}O_{seawater}$ values appears to be independent of the materials studied and is recorded by carbonates, silica, brachiopods, and conodonts. An alternative interpretation of the data is that $\delta^{18}O_{seawater}$ has largely remained constant at ~ -0.8 to +1.4‰ and is controlled by ice volumes. The higher inferred temperatures derived from very old rocks are purported to be an artifact of preservation (Finnegan et al., 2011; Henkes et al., 2018). Opinions are still divided, and consensus is far from reached. For further information on this paleothermometer and stable isotope geochemistry in general, see Sharp (2017).

3.4.2. Trace Metal Paleothermometry

Two important trace metal thermometers have been developed over the past decades: Mg/Ca of (primarily) planktic foraminifers, which is explored here, and Sr/Ca of coral aragonite. The Mg/Ca temperature proxy derives from the substitution of Mg^{2+} for Ca into biogenic calcite (first recognized by Chave, 1954). The rate of this substitution is dependent on the temperature of the seawater from which calcifiers precipitate their tests, such that Mg/Ca increases with increasing temperature. Since the mid-1990s, Mg/Ca, particularly in planktic foraminifers, has become widely, almost routinely, used, especially following the development of species-specific Mg/Ca versus temperature relationships (Nürnberg et al., 1996; see also the review of Barker et al., 2005). The technique has also been successfully performed using other calcifiers such as benthic foraminifers (Elderfield & Ganssen, 2000; Lear et al., 2000), nonmarine (Chivas et al., 1987) and marine (Dwyer et al., 2002) ostracods, and corals (Mitsuguchi et al., 1996). Calibration of Mg/Ca versus temperature has been carried out for several (extant) species of planktic foraminifera using core-top, culture, and sediment trap studies, in which Mg/Ca is calculated from recent specimens either grown in or taken from conditions with known parameters (for further details see Barker et al., 2005). The Mg/Ca method is now refined to the extent that it can be used to reconstruct past temperatures to within <1°C error, and as such it is a very powerful part of the paleoceanographer's toolbox.

Advantages of Mg/Ca paleothermometry include an ability to reconstruct temperatures from different depths in the water column depending on the habitat preferences of the studied species, and the relative ease of performing

elemental analyses, such that high- resolution records can be generated fairly quickly. The relatively long oceanic residence times of Ca (10^6 y) and Mg (10^7 y) implies that, unlike $\delta^{18}O_{seawater}$, the Mg/Ca ratio of seawater is likely constant over glacial/interglacial timescales and through transitions between these climatic states. Furthermore, trace metal proxies can be paired with $\delta^{18}O$ analyses on the same shells to provide information on both sea-surface temperatures (SST) and the $\delta^{18}O$ composition of seawater (e.g., Lea et al., 2000). However, as with all methods, trace metal paleothermometry has its limitations. Thus, pH and salinity also influence the incorporation of Mg^{2+} into calcite. These factors have opposing effects: seawater pH negatively correlates with Mg^{2+} uptake, while salinity has a positive relationship (Nürnberg et al., 1996; Kisakürek et al., 2008). Care must be taken when interpreting Mg/Ca records through intervals that might have experienced changes in either or both pH and salinity. A further complication is that calcite dissolution can preferentially remove relatively soluble high-Mg shell material (Brown & Elderfield, 1996) limiting the use of Mg/Ca paleothermometry in cases where dissolution is suspected. Perhaps the most significant drawback associated with trace-metal paleothermometry is that the aforementioned factors, plus the fact that high-Mg calcite is metastable during diagenesis, determine that the Mg/Ca method cannot be employed in material much older than the Cenozoic.

3.4.3. Biomarker Paleothermometry

Biomarker paleothermometry is based on the compositions of biologically mediated long-chain organics, which are often governed by the growth temperature of microbes. Biomarker thermometers such as TEX_{86} and alkenones are powerful tools for reconstructing SSTs and have been applied in many paleoenvironmental studies of marine and lacustrine sediments (e.g., Zachos et al., 2006).

TEX_{86} is an abbreviation for the tetraether index of 86 carbon atoms and is based upon the glycerol dialkyl glycerol tetraethers (GDGTs) of the marine archaea Thaumarchaeota (Schouten et al., 2002). GDGTs are the main components of Thaumarchaeota membrane lipids and contain cyclopentane moieties. The degree of cyclization is generally governed by growth temperature. In its favor, and in contrast to some other proxies, TEX_{86} is not influenced by freshwater input or salinity changes. Due to the complexity of biochemical processes, the proxy has two main calibrations against SST: TEX_{86}^{H} for temperatures above 15°C and TEX_{86}^{L} for temperatures below 15°C (see Kim et al., 2010, for details).

Higher burial temperatures can offset TEX_{86} to higher inferred temperatures, and since the long-chain organics are readily broken into short-chain compounds at high temperatures, biomarker paleothermometry is rarely successful in pre-Cretaceous studies. The oldest strata in which TEX_{86} has been employed is of Early Jurassic age (Robinson et al., 2017). Since GDGTs also occurred globally in soils, high terrestrial organic carbon input can substantially bias TEX_{86}-reconstructed sea and lake surface temperatures (Weijers et al., 2006).

Alkenones are long-chain unsaturated methyl and ethyl *n*-ketones produced by a few phytoplanktic coccolithophorids. Alkenone thermometry (also known as the alkenone unsaturation index) involves measuring changes in the degree of unsaturation and in the overall carbon chain length distribution of alkenones as well as the proportion of fatty acid esters relative to alkenones (Prahl et al., 1988). As much as 85% of the total alkenones are degraded over ~8 kyr as a consequence of diffusion-controlled oxidation, but the degradative loss has little effect on the unsaturation pattern of remaining alkenones (Prahl et al., 1989). As with TEX_{86}, the alkenone proxy requires distinct temperature calibrations specific to the environment of deposition. This is largely due to difficulties in disentangling systems harboring different alkenone-producing haptophyte species and restricts applications in saline lakes and marginal ocean environments (see Zheng et al., 2019, for details). The oldest preserved alkenones are of Early Cretaceous age (Brassell & Dumitrescu, 2004), and thus this is the limit of their application in paleothermometry.

3.4.4. Clumped-Isotope Paleothermometry

This novel technique holds that the abundance of the double substituted CO_2 isotopologue, $^{13}C^{18}O^{16}O$ is proportional to the abundance of ^{13}C-^{18}O bonds in carbonate, and is a function of temperature (Ghosh et al., 2006; Eiler, 2007). Unlike "conventional" $\delta^{18}O$ paleothermometry, clumped-isotope thermometry is based on internal bond ordering rather than bulk isotopic composition. Thus, the great advantage of the method is that when combined with conventional $\delta^{18}O_{carbonate}$, clumped isotopes simultaneously provide temperature data as well as $\delta^{18}O_{seawater}$ values. The evidence for a relatively constant Phanerozoic $\delta^{18}O_{seawater}$ (see section 3.4.1.2) mostly derives from clumped isotopes (Henkes et al., 2018). Early measuring protocols and instrument setups generally required between 4 and 15 mg of powdered sample material, and a long integration time, meaning that measurements were time consuming. However, recent advances have greatly reduced the weight of required sample material required by a factor of ~40 times to 90 μg, and instruments can reach the same levels of analytical precision in a much shorter time, revealing the great potential of clumped-isotope paleothermometry on, for example, rare materials

(Müller et al., 2017). Despite these apparent benefits and recent advances, clumped-isotope thermometry remains a developing field because solid-state diffusion of carbon and oxygen in carbonate can affect the reliability of results. Differences in approaches between laboratories worldwide have yet to be reconciled, but clumped-isotope paleothermometry has an exciting future.

3.5. TWO GREAT HOTHOUSES IN EARTH HISTORY

3.5.1. The Permian-Triassic Super Greenhouse

The greatest extinction in Earth history, at the Permian-Triassic boundary, saw the loss of >90% of marine species (e.g., Erwin, 1994), widespread devastation on land (e.g., Retallack, 1995; Smith & Ward, 2001), and the only recorded mass extinction of the seemingly indomitable insects (Labandeira & Sepkoski, 1993). This transition is associated with the greatest episode of global warming of the Phanerozoic (Fig. 3.4), surely more than mere coincidence? Extensive damage was done to both terrestrial and marine ecosystems in a relatively brief interval of geological time (perhaps as short as a few thousands of years). Thus, the extinction interval has been constrained radio-isotopic dating of ash beds to between 251.941 ± 0.037 and 251.880 ± 0.031 Mya, an interval of just 60 ± 48 kyr (Burgess et al., 2014). The onset of extinctions coincides almost perfectly with the beginning of the second phase of Siberian Traps volcanism (the onset of widespread Siberian Traps sill emplacement), which is dated to 251.907 ± 0.067 Ma (Burgess et al., 2017). Postulated kill mechanisms include marine anoxia, volcanic winter, hypercapnia, ocean acidification, eutrophication driven by increased sediment flux to the oceans, ozone destruction, extreme atmospheric oxygen depletion, poisoning by toxic trace metals, and of course, global warming (see reviews of Benton & Twitchett, 2003; Racki & Wignall, 2005; Wignall, 2007; Bond & Wignall, 2014; Wignall, 2015; Bond & Grasby, 2017). As discussed earlier, these were driven by the eruptions of the Siberian Traps, with additional contributions of greenhouse gases and other deadly volatiles likely coming from contact metamorphism of high-level organic-rich sediments (e.g., Svensen et al., 2009).

Many of the stresses implicated in the Permian-Triassic crisis are synergistic, but two in particular go hand-in-hand: marine anoxia and warming. There is abundant facies and geochemical evidence for the development of widespread marine anoxia across the Permian-Triassic boundary (Bond & Grasby, 2017). Anoxia is a function of warming oceans that dissolve oxygen (and other gases) less readily. The Permian-Triassic has long been a focus of paleothermometry and the earliest $\delta^{18}O$ records invoked warming of "perhaps 5°C" (Holser et al., 1989, p. 41). More recently, groundbreaking high-resolution conodont apatite oxygen isotope studies have revealed a far more significant rise in sea surface temperatures during the extinction interval (e.g., Joachimski et al., 2012; Sun et al., 2012). Rapid warming, from 21° to 36°C, occurred over ~0.8 million years across the Permian-Triassic boundary, around 13°C of which took place in the final 500,000 years of the Permian (Sun et al., 2012; Fig. 3.4). The global hothouse climaxed when equatorial seas reached temperatures around 37°C in the upper water column during the Griesbachian (the earliest substage of the Triassic; ~252.1 Ma). Sea-surface temperatures were likely 2–3°C warmer. Such warmth is thought to have been inimical to life in the oceans: many marine groups, particularly those with a high metabolism, cannot survive temperatures above 35°C for long (Pürtner, 2002), although some, such as ostracods and gastropods, tolerate higher temperatures than others, such as corals, cephalopods, and foraminifera (Song et al., 2014). The added stress of oxygen deficiency, which was not ubiquitous, and therefore cannot have been the sole killer, cannot have helped, leading to suggestions that marine taxa were stuck between a rock and a hard place during the latest Permian, the "anoxia / high temperature double whammy" scenario of Song et al. (2014). It probably got even hotter on land, where temperatures might have reached >40°C in the tropics (Sun et al., 2012). Few plants can survive such heat (Ellis, 2010) and thus extreme warming is a compelling extinction mechanism not only for the oceanic scenario but also for the collapse of terrestrial ecosystems across the Permian-Triassic boundary. It is worth noting here that almost all data on Permian-Triassic seawater temperatures derive from studies of equatorial latitudes. While it seems likely that the entire world experienced this deadly heat wave, modeling suggests that at a regional scale, changes in paleogeography alone can cause temperature changes on the order of 10°C, which have little relationship with global average temperature change (Lunt et al., 2016). Refining our understanding of global temperature changes during the crisis interval, and in particular reconstructing latitudinal temperature gradients, is the subject of our ongoing work.

3.5.2. Paleocene-Eocene Thermal Maximum

Around 56 Myr ago, longer term warming that began in the late Paleocene was punctuated by a rapid 4–5°C temperature rise associated with a 3–6‰ negative carbon isotope shift (Jones et al., 2013). This, the most recent example of intense global warming, resulted in the Paleocene-Eocene Thermal Maximum (PETM). Despite the relative youth of the PETM, its cause, duration, timing, magnitude, and effects remain controversial

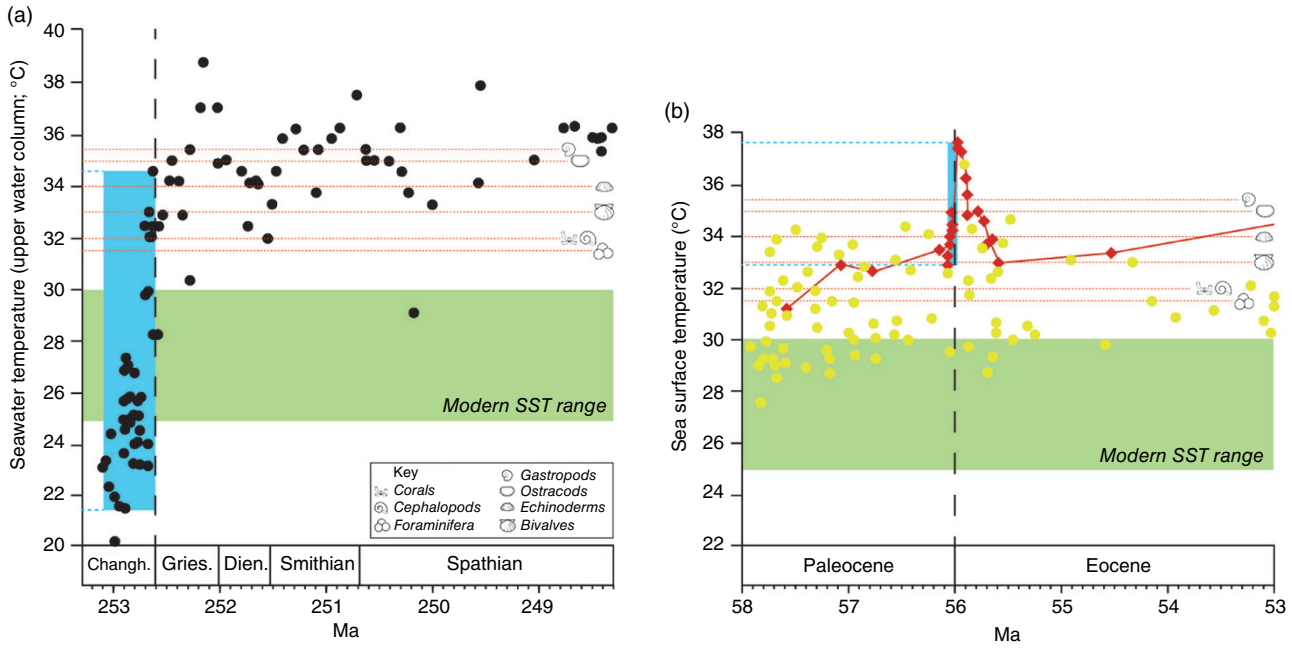

Figure 3.4 Comparison of low-latitude warming trends across the Permian-Triassic boundary and Paleocene-Eocene boundary. The time and temperature axes are the same scale in both panels (a) and (b) allowing direct comparison of these two major global warming episodes. Similar maximum temperatures are attained during both events, although high temperatures were sustained for a longer duration in the Early Triassic than in the early Eocene. The range of modern equatorial sea-surface temperatures (SSTs) is shown by the green box in each panel. The red dotted lines on each panel represent the median upper thermal lethal limits for selected (modern) marine faunal groups, based on a database compiled by Song et al. (2014). Permian-Triassic warming followed a relatively cool interval, whereas its Paleocene-Eocene counterpart was imprinted on already warm conditions. Panel (a) shows a ca. 13°C warming in equatorial ocean temperatures during the 500,000 years leading up to the Permian-Triassic boundary and contemporaneous mass extinction (represented by blue box and dashed lines; equating to approximately 2.6°C per 100,000 years). This temperature record is based on oxygen isotopes of conodont apatite samples from South China and includes data from a 5 Myr interval between 253.3 Ma and 248.3 Ma (timescale of Gradstein et al., 2012) taken from Sun et al. (2012). Inferred paleotemperatures exceed the median lethal limits for most groups at the Permian-Triassic boundary, and the sustained Early Triassic hothouse is considered a factor in the delayed recovery from extinction (Sun et al., 2012). Changh. = Changhsingian (Permian); Gries. = Griesbachian (Triassic); Dien. = Dienerian. Panel (b) shows a more rapid, but smaller scale warming of ca. 4.5°C in the 100,000 years prior to the Paleocene-Eocene boundary (blue box and dashed lines) including data from a 5 Myr interval between 58 Ma and 53 Ma (timescale of Gradstein et al., 2012). Yellow circles = tropical Paleocene-Eocene sea-surface temperature estimates based on the $\delta^{18}O$, Mg/Ca and TEX-86 proxies compiled by Cramwinckel et al. (2018) using data from Tripati et al. (2003), Pearson et al. (2007, 2008), Lear et al. (2008), Liu et al. (2009), Aze et al. (2014), Inglis et al. (2015), Frieling et al. (2017), and Evans et al. (2018); red diamonds = equatorial sea-surface temperatures inferred from biomarker paleothermometry (TEX_{86}) of Atlantic Ocean IODP Site 959 sediments (Cramwinckel et al., 2018; Frieling et al., 2018). Intriguingly, inferred temperatures at the Paleocene-Eocene boundary exceed the median lethal limits for all groups shown here, and yet this event is associated with comparatively low extinction rates. This suggests that either the preexisting climate state plays an important role in the lethality of warming, or that modern biota are more tolerant of warming than their Paleozoic counterparts (or both).

(McInerney & Wing, 2011; Bowen et al., 2015). This event, and one of several postulated drivers (the North Atlantic Igneous Province; e.g., Eldholm & Thomas, 1993) are examined elsewhere in this volume. Here we briefly summarize the details of warming for comparison with the Permian-Triassic.

Quantitative comparison of paleotemperature proxy data with fully coupled climate model simulations suggests global average temperatures reached about 29°C in the early Eocene. For context, the modern preindustrial global average sea temperature was 14.4°C (Cramwinckel et al., 2018). The rate of warming (ca. 5°C in low

latitudes; 8°C in high latitudes) is debated, but a recent summary (Cramwinckel et al., 2018) of TEX_{86} data indicated that most of the warming occurred in <100,000 years in the latest Paleocene (Fig. 3.4). Tropical surface and deep-ocean records reveal synchronous temperature changes on both short-term and long-term timescales, suggesting that greenhouse gas forcing rather than ocean circulation changes were responsible for warming (Anagnostou et al., 2016; Cramwinckel et al., 2018). The source of this greenhouse gas is controversial; several authors invoke destabilization of carbon from surface sedimentary reservoirs such as methane hydrates (e.g., Dickens et al., 1995) that was triggered by initial deep-sea warming due to volcanogenic CO_2 (Thomas & Shackleton, 1996). Others consider that the observed carbon isotope shifts can only be reconciled with large igneous province eruptions in the North Atlantic (Gutjahr et al., 2017). Estimates of the total carbon budget for the PETM range from 3,000 to 10,000 Gt (the upper estimate equivalent to a mass of 37,000 Gt CO_2; Zeebe et al., 2009; Cui et al., 2011), all of which was released over thousands (Zeebe et al., 2014) to tens of thousands of years (Cui et al., 2011), or longer (see Turner, 2018, for a review). Bowen et al.'s (2015) carbon cycle model suggests that the beginning of the PETM saw two major pulses of atmospheric carbon injections separated by a recovery to background emissions. Their first pulse had an estimated loading of around 1 Gt carbon per year for around 2000 years; huge, but still an order of magnitude smaller than the current anthropogenic input.

Curiously, the PETM is not associated with widespread extinctions, despite Earth's tropical oceans attaining temperatures similar to those postulated for the catastrophic Permian-Triassic world (Fig. 3.4). The most significant victims were deeper-water benthic foraminifera, which suffered 30%–50% species loss (Thomas, 1998). Shallow waters experienced the loss of reef facies in Tethys during the crisis (Scheibner & Speijer, 2008) although these reappeared in the Eocene with the same genera. Planktic foraminifera actually diversified during the PETM (e.g., Kelly et al., 1998), and calcareous nannoplankon mostly also enjoyed the warm conditions. The missing extinction conundrum is explained through regional studies: Aze et al. (2014) document a site in Tanzania where calcareous nannoplankton and foraminifers disappear for the entire PETM as SSTs likely exceeded 40°C; Frieling et al. (2017) estimate similar SSTs for a site in Nigeria where dinocyst abundance and diversity plummets at the peak of the PETM. Where it was bad, it was bad, but conditions simply did not get inimical enough, widely enough, to do significant harm to ecosystems. The absence of widespread anoxia at the PETM might also factor in its apparent nonlethality. Some have invoked widespread ocean acidification, a consequence of increased atmospheric CO_2, in the benthic losses (e.g., Zachos et al., 2005), but this is still to be reconciled with observed extinction patterns. Clearly numerous factors must influence the biotic impact of global warming.

3.5.3. Key Factors: Why Does Warming Sometimes Kill and Sometimes Does Not?

Many factors must influence the capacity of a LIP to drive environmental change and the ecological effects of global warming. These might include initial (background) climate conditions, perhaps the key to the PETM's nonlethality, where extant taxa were already adapted to warmth, in contrast to the end-Permian catastrophe, which followed a prolonged interval of cool conditions, continental configuration, and the innate resilience of the extant biota to change or its ability to migrate to more habitable regions. The rate and/or magnitude of global warming might be an important factor. Thus, the half-million years before the Permian-Triassic boundary experienced warming of ca. 13°C at an average rate of 2.6°C per 100,000 years. The PETM was the manifestation of ca. 5°C warming in not more than (and possibly much less than) 100,000 years, and although the rate of PETM warming was faster, the absolute magnitude of this change was markedly less than that during the Permian-Triassic transition. Of the many factors above, Wignall (2015) concluded that the presence/absence of Pangea was a defining factor in determining LIP lethality. Certainly of the post-Pangean LIPs, only one (the Deccan Traps) is associated with a major extinction, and that is complicated by the meteorite impact at the Cretaceous-Paleogene boundary. Zaffos et al. (2017) compared marine animal diversity with continental configuration and concluded that variations in diversity since the Ordovician are due to the assembly and disassembly of the Pangea. Continental configuration might also affect the silicate weathering cycle, which Kump (2018) suggests is a positive feedback loop that regulates climate. Thus, increased atmospheric CO_2 leads to warming and enhanced precipitation, which leads to elevated silicate weathering and CO_2 drawdown (e.g., Dickson et al., 2015; Penman, 2016). In the PETM scenario, the continents were configured such that silicate weathering could get climate in check relatively quickly; in the Early Triassic, it could not, resulting in a failure of the system to ameliorate warming for several millions of years (Kump, 2018).

There are clearly numerous variables that influence the LIP-warming-extinction link and many of these are yet to be properly evaluated. There are doubtless several more that we have not even thought of. Improved understanding of these synergies is vital in light of the looming Anthropocene crisis. Will the existence of the calcareous nannoplankton (for example), absent from the Permian

world, but now keeping our carbon cycle in check through their very own carbon capture and storage, save us in the Anthropocene? They did not prevent climate change during the PETM. We really do not know what the future holds, but this is not an excuse for complacency over the coming decades; indeed, quite the opposite.

3.6. GLOBAL WARMING IN THE ANTHROPOCENE

The Anthropocene concept is explored elsewhere in this volume, but a brief comparison of past crises with the modern provides some interesting, and worrying, food for thought with which to conclude this chapter. The worst-case global warming scenario put forward by the Intergovernmental Panel on Climate Change (IPCC) predicts a global sea-water temperature rise of 6.4°C by the year 2100 (IPCC, 2013). This is astonishing, given that paleothermometry suggests that some ancient crises were associated with similar warming episodes (over much longer timescales), such as 4°C at the Cretaceous-Paleogene boundary (Li & Keller, 1998; Wilf et al., 2003) and 7°C in the Late Devonian (Joachimski et al., 2009), but the forecast warming is some way short of the 13–15°C across the Permian-Triassic boundary (Sun et al., 2012). Predicting the effects of warming is not made easier by episodes such as the PETM, during which a 5°C rise that led to equatorial temperatures exceeding the upper lethal limits for most taxa (Fig. 3.4) had surprisingly little effect on biodiversity. Nevertheless, the latest IPCC special report (IPCC, 2018), which focuses on limiting global warming in the coming decades to 1.5°C, highlights just how damaging exceeding this threshold could be, with eye-catching predictions that coral reefs will decline by 70–90% if sea-surface temperatures rise by 1.5°C, increasing to >99% in a 2°C warming scenario. Modern warming, like its ancient equivalents, is largely being driven by rising atmospheric CO_2. In the 18 years between October 2000 and October 2018, atmospheric CO_2 has increased from ~367 ppm to ~407 ppm (Scripps, 2018), a net rise of 40 ppm (2.22 ppm/y). This is equivalent to the addition of ~17 Gt CO_2 *every year*, and the rate of addition is accelerating rapidly, because anthropogenic CO_2 release is now 37 Gt per year. Perhaps not coincidentally, the United Kingdom's 10 warmest years have all occurred since 2002 (Kendon et al., 2019), a pattern being played out globally. According to Courtillot and Renne (2003), the Siberian Traps, which generated the greatest hothouse in Earth history, injected 30,000 Gt of CO_2 into the Permian atmosphere. At today's rate of anthropogenic emissions, it would take only 800 years to inject that mass of CO_2. It would take only 4,600 years to inject as much CO_2 as Sobolev et al.'s (2011) far-higher estimate of Siberian Traps of 170,000 Gt, which incorporated recycled ocean crust into the ascending plume. As geologists perhaps uniquely understand, a few thousand years is truly a geological instant. We still do not know if it is the magnitude of warming, the rate of warming (e.g., Fig. 3.4), or some other factor(s) that govern life's response to climate change. Given this lack of security in our future, society in general needs to learn from these past episodes of global warming in order to understand the present crisis. As we know, if it has happened before, then it can happen again.

ACKNOWLEDGMENTS

DB acknowledges Natural Environment Research Council (NERC; grant number NE/J01799X/1), which supported his time while writing this chapter. YS acknowledges the Deutsche Forschungsgemeinschaft (DFG, German Science Foundation) Research Unit TERSANE (FOR 2332: Temperature-related stressors as a unifying principle in ancient extinctions; Project 219/15), and the National Natural Science Foundation of China (41602026, 41821001).

REFERENCES

Aldridge, R. J., & Purnell, M. A. (1996). The conodont controversies. *Trends in Ecology & Evolution*, *11*(11), 463–468.

Algeo, T. J., & Scheckler, S. E. (1998). Terrestrial-marine teleconnections in the Devonian: Links between the evolution of land plants, weathering processes, and marine anoxic events. *Philosophical Transactions of the Royal Society of London. Series B: Biological Sciences*, *353*, 113–130.

Algeo, T. J., & Twitchett, R. J. (2010). Anomalous Early Triassic sediment fluxes due to elevated weathering rates and their biological consequences. *Geology*, *38*, 1023–1026.

Algeo, T. J., Berner, R. A., Maynard, J. B., & Scheckler, S. E. (1995). Late Devonian oceanic anoxic events and biotic crises:Rooted in the evolution of vascular land plants. *GSA Today*, *5*, 45–66.

Anagnostou, E., John, E. H., Edgar, K. M., Foster, G. L., Ridgwell, A., Inglis, G. N., et al. (2016). Changing atmospheric CO_2 concentration was the primary driver of early Cenozoic climate. *Nature*, *533*, 380–384.

Archer, D. (2005). Fate of fossil fuel CO_2 in geologic time. *Journal of Geophysical Research: Oceans*, *110*, C09S05.

Aze, T., Pearson, P. N., Dickson, A. J., Badger, M. P., Bown, P. R., Pancost, R. D., Gibbs, S. J., et al. (2014). Extreme warming of tropical waters during the Paleocene-Eocene Thermal Maximum. *Geology*, *42*, 739–742.

Barker, S., Cacho, I., Benway, H., & Tachikawa, K. (2005). Planktonic foraminiferal Mg/Ca as a proxy for past oceanic temperatures: A methodological overview and data compilation for the Last Glacial Maximum. *Quaternary Science Reviews*, *24*, 821–834.

Benton, M. J., & Twitchett, R. J. (2003). How to kill (almost) all life: The end-Permian extinction event. *Trends in Ecology and Evolution*, *18*, 358–365.

Berner, R. A. (2002). Examination of hypotheses for the Permo-Triassic boundary extinction by carbon cycle modeling. *Proceedings of the National Academy of Sciences of the United States of America*, *99*, 4172–4177.

Black, B. A., Lamarque, J.-F., Shields, C. A., Elkins-Tanton, L. T., & Kiehl, J. T. (2014). Acid rain and ozone depletion from pulsed Siberian Traps magmatism. *Geology*, *42*, 67–70.

Bond, D. P. G., & Grasby, S. E. (2017). On the causes of mass extinctions. *Palaeogeography, Palaeoclimatology, Palaeoecology*, *478*, 3–29.

Bond, D. P. G., & Wignall, P. B. (2014). Large igneous provinces and mass extinctions: An update. *Geological Society of America Special Papers*, *505*, SPE 505–02.

Bond, D., Wignall, P. B., & Racki, G. (2004.) Extent and duration of marine anoxia during the Frasnian-Famennian (Late Devonian) mass extinction in Poland, Germany, Austria, and France. *Geological Magazine*, *141*, 173–193.

Bowen, G. J., Maibauer, B. J., Kraus, M. J., Röhl, U., Westerhold, T., Steimke, A., et al. (2015). Two massive, rapid releases of carbon during the onset of the Palaeocene-Eocene thermal maximum. *Nature Geoscience*, *8*(1), 44.

Brassell, S. C., & Dumitrescu, M. (2004). Recognition of alkenones in a lower Aptian porcellanite from the west-central Pacific. *Organic Geochemistry*, *35*, 181–188.

Briffa, K. R., Schweingruber, F. H., Jones, P. D., Osborn, T. J., Shiyatov, S. G., & Vaganov, E. A. (1998). Reduced sensitivity of recent tree-growth to temperature at high northern latitudes. *Nature*, *391*, 678–682.

Brown, S. J., & Elderfield, H., (1996). Variations in Mg/Ca and Sr/Ca ratios of planktonic foraminifera caused by postdepositional dissolution: Evidence of shallow Mg dependent dissolution. *Paleoceanography*, *11*, 543–551.

Bryan, S. E., & Ernst, R. E. (2008). Revised definition of large igneous provinces (LIPs). *Earth Science Reviews*, *86*, 175–202.

Burgess, S. D., Bowring, S., & Shen, S.-Z. (2014). High-precision timeline for Earth's most severe extinction. *Proceedings of the National Academy of Sciences of the United States of America*, *111*, 3316–3321.

Burgess, S. D., Muirhead, J. D., & Bowring, S. A. (2017). Initial pulse of Siberian Traps sills as the trigger of the end-Permian mass extinction. *Nature Communications*, *8*, 164.

Chave, K. E. (1954). Aspects of the biogeochemistry of magnesium 1. Calcareous marine organisms. *The Journal of Geology*, *62*, 266–283.

Chivas, A. R., De Deckker, P., & Shelley, J. M. G. (1987). Magnesium and strontium in non-marine ostracod shells as indicators of palaeosalinity and palaeotemperature. *Paleolimnology IV*, 135–142.

Cicerone, R. J., & Oremland, R. S. (1988). Biogeochemical aspects of atmospheric methane. *Global Biogeochemical Cycles*, *2*, 299–327.

Cossins, A. R., & Bowler, K. (1987). *Temperature biology of animals*. New York, NY: Chapman and Hall.

Courtillot, V. E., & Renne, P. R. (2003). On the ages of flood basalt events. *Comptes Rendus Geosciences*, *335*, 113–140.

Cramwinckel, M. J., Huber, M., Kocken, I. J., Agnini, C., Bijl, P. K., Bohaty, S. M., et al. (2018). Synchronous tropical and polar temperature evolution in the Eocene. *Nature*, *559*, 382–386.

Cui, Y., Kump, L. R., Ridgwell, A. J., Charles, A. J., Junium, C. K., Diefendorf, A. F., et al. (2011). Slow release of fossil carbon during the Palaeocene-Eocene Thermal Maximum. *Nature Geoscience*, *4*, 481–485.

Deegan, F. M., Troll, V. R., Bédard, J. H., Evenchick, C. A., Dewing, K., Grasby, S., et al. (2016). The stiff upper LIP: investigating the High Arctic Large Igneous Province. *Geology Today*, *32*, 92–98.

Diaz, R. J., & Rosenberg, R. (1995). Marine benthic hypoxia: A review of its ecological effects and the behavioural responses of benthic macrofauna. *Oceanography and Marine Biology*. *An Annual Review*, *33*, 245–03.

Dickens, G. R. (1999). Carbon cycle: The blast in the past. *Nature*, *401*, 752–755.

Dickens, G. R., Castillo, M. M., & Walker, J. C. G. (1997). A blast of gas in the latest Paleocene: Simulating first-order effects of massive dissociation of oceanic methane hydrate. *Geology*, *25,* 259–262.

Dickens, G. R., O'Neil, J. R., Rea, D. K., & Owen, R. M. (1995). Dissociation of oceanic methane hydrate as a cause of the carbon isotope excursion at the end of the Paleocene. *Paleoceanography and Paleoclimatology*, *10*, 965–971.

Dickson, A. J., Cohen, A. S., Coe, A. L., Davies, M., Shcherbinina, E. A., & Gavrilov, Y. O. (2015). Evidence for weathering and volcanism during the PETM from Arctic Ocean and Peri-Tethys osmium isotope records. *Palaeogeography, Palaeoclimatology, Palaeoecology*, *438*, 300–307.

Dwyer, G. S., Cronin, T. M., & Baker, P. A. (2002). Trace elements in marine ostracodes. *American Geophysical Union Geophysical Monograph, 131*, 205–226.

Eiler, J. M. (2007). "Clumped-isotope" geochemistry: The study of naturally-occurring, multiply-substituted isotopologues. *Earth and Planetary Science Letters*, *262*(3–4): 309–327.

Elderfield, H., & Ganssen, G. (2000). Past temperature and $\delta^{18}O$ of surface ocean waters inferred from foraminiferal Mg/Ca ratios. *Nature*, *405*, 442.

Eldholm, O., & Thomas, E. (1993). Environmental impact of volcanic margin formation. *Earth and Planetary Science Letters*, *117*, 319–329.

Ellis, R. J. (2010). Biochemistry: Tackling unintelligent design. *Nature*, *463*, 164–165.

Ernst, R. E., & Youbi, N. (2017). How Large Igneous Provinces affect global climate, sometimes cause mass extinctions, and represent natural markers in the geological record. *Palaeogeography, Palaeoclimatology, Palaeoecology*, *478*, 30–52.

Erwin, D. H. (1994). The Permo-Triassic extinction. *Nature*, *367*, 231–236.

Evans, D., Sagoo, N., Renema, W., Cotton, L. J., Müller, W., Todd, J. A., Saraswati, P. K., et al. (2018). Eocene greenhouse climate revealed by coupled clumped isotope-Mg/Ca thermometry. *Proceedings of the National Academy of Sciences*, *115*, 1174–1179.

Finnegan, S., Bergmann, K., Eiler, J. M., Jones, D. S., Fike, D. A., Eisenman, I., et al. (2011). The Magnitude and duration of Late Ordovician-Early Silurian glaciation. *Science*, *331*, 903–906.

Foster, G. L., Hull, P., Lunt, D. J., & Zachos, J. C. (2018). Placing our current "hyperthermal" in the context of rapid

climate change in our geological past. *Philosophical Transactions. Series A, Mathematical, Physical, and Engineering Sciences*, *376*, 2130.

Frederich, M., & Pörtner, H. O. (2000). Oxygen limitation of thermal tolerance defined by cardiac and ventilatory performance in spider crab, *Maja squinado*. *American Journal of Physiology: Regulatory, Integrative and Comparative Physiology*, *279*, R1531–R1538.

Frieling, J., Gebhardt, H., Huber, M., Adekeye, O. A., Akande, S. O., Reichart, G. J., Middelburg, J. J., et al. (2017). Extreme warmth and heat-stressed plankton in the tropics during the Paleocene-Eocene Thermal Maximum. *Science Advances*, *3*, p.e1600891.

Frieling, J., Reichart, G. J., Middelburg, J. J., Röhl, U., Westerhold, T., Bohaty, S. M., & Sluijs, A. (2018). Tropical Atlantic climate and ecosystem regime shifts during the Paleocene-Eocene Thermal Maximum. *Climate of the Past*, *14*, 39–55.

Frieling, J., Svensen, H. H., Planke, S., Cramwinckel, M. J., Selnes, H., & Sluijs, A. (2016). Thermogenic methane release as a cause for the long duration of the PETM. *Proceedings of the National Academy of Sciences*, *113*, 12059–12064.

Ghosh, P., Adkins, J., Affek, H., Balta, B., Guo, W., Schauble, E. A., et al. (2006). ^{13}C-^{18}O bonds in carbonate minerals: A new kind of paleothermometer. *Geochimica et Cosmochimica Acta*, *70*(6), 1439–1456.

Gradstein, F. M, Ogg, J. G., Schmitz, M., & Ogg, G. (2012). *The geologic time scale* 2012. Amsterdam, Netherlands: Elsevier.

Grasby, S. E., Beauchamp, B., & Knies, J. (2016). Early Triassic productivity crises delayed recovery from world's worst mass extinction. *Geology*, *44*, 779–782.

Grasby, S. E., Knies, J., Beauchamp, B., Bond, D. P. G., Wignall, P. B., & Sun, Y. (2020). Global warming leads to Early Triassic nutrient stress across northern Pangea. *Geological Society of America Bulletin, 132*(5–6), 943–954. https://doi.org/10.1130/B32036.1

Grasby S. E., Sanei, H., & Beauchamp B. (2011). Catastrophic dispersion of coal fly ash into oceans during the latest Permian extinction. *Nature Geoscience*, *4*, 104–107.

Gutjahr, M., Ridgwell, A., Sexton, P. F., Anagnostou, E., Pearson, P. N., Pälike, H., et al. (2017). Very large release of mostly volcanic carbon during the Palaeocene–Eocene Thermal Maximum. *Nature*, *548*, 573–577.

Harkness, D. D., Gaunt, G. D., & Nunney, J. H. (1976). Radiocarbon dating versus the Leeds Hippopotamus: A cautionary tale. *Proceedings of the Yorkshire Geological Society*, *41*(2), 223–230.

Henkes, G. A., Passey, B. H., Grossman, E. L., Shenton, B. J., Yancey, T. E., & Pérez-Huerta, A. (2018). Temperature evolution and the oxygen isotope composition of Phanerozoic oceans from carbonate clumped isotope thermometry. *Earth and Planetary Science Letters*, *490*, 40–50.

Holser, W. T., Schönlaub, H. P., Attrep, M. Jr., Boeckelmann, K., Klein, P., Magaritz, M., et al. (1989). A unique geochemical record at the Permian/Triassic boundary. *Nature*, *337*, 39–44.

Inglis, G. N., Farnsworth, A., Lunt, D., Foster, G. L., Hollis, C. J., Pagani, M., Jardine, P. E., et al. (2015). Descent toward the Icehouse: Eocene sea surface cooling inferred from GDGT distributions. *Paleoceanography*, *30*, 1000–1020.

IPCC (2013). *Climate change 2013: The physical science basis*. Contribution of Working Group I to the Fifth Assessment Report of the Intergovernmental Panel on Climate Change. Cambridge and New York: Cambridge University Press.

IPCC (2014). *Climate change 2014: Synthesis report*. Contribution of Working Groups I, II and III to the Fifth Assessment Report of the Intergovernmental Panel on Climate Change. IPCC.

IPCC (2018). *Global warming of 1.5°C*. Special Report 15. http://www.ipcc.ch/report/sr15/

Jaffrés, J. B. D., Shields, G. A., & Wallmann, K. (2007). The oxygen isotope evolution of seawater: A critical review of a long-standing controversy and an improved geological water cycle model for the past 3.4 billion years. *Earth-Science Reviews*, *83*(1–2), 83–122.

Joachimski, M. M., Breisig, S., Buggisch, W., Talent, J. A., Mawson, R., Gereke, M., et al. (2009). Devonian climate and reef evolution: Insights from oxygen isotopes in apatite. *Earth and Planetary Science Letters*, *284*, 599–609.

Joachimski, M. M., Lai, X.-L., Shen, S.-Z., Jiang, H.-S., Luo, G.-M., Chen, B., et al. (2012). Climate warming in the latest Permian and the Permian-Triassic mass extinction. *Geology*, *40*, 195–198.

Jones, M. T., Jerram, D. A., Svensen, H. H., & Grove, C. (2016). The effects of large igneous provinces on the global carbon and sulphur cycles. *Palaeogeography, Palaeoclimatology, Palaeoecology*, *441*, 4–21.

Jones, T. D., Lunt, D. J., Schmidt, D. N., Ridgwell, A., Sluijs, A., Valdes, P. J., & Maslin, M. (2013). Climate model and proxy data constraints on ocean warming across the Paleocene-Eocene Thermal Maximum. *Earth-Science Reviews*, *125*, 123–145.

Jugo, P. J., Luth, R. W., & Richards, J. P. (2005). An experimental study of the sulfur content in basaltic melts saturated with immiscible sulfide or sulfate liquids at 1300° C and 1· 0 GPa. *Journal of Petrology*, *46*(4), 783–798.

Katz, M. E., Pak, D. K., Dickens, G. R., & Miller, K. G. (1999). The source and fate of massive carbon input during the latest Paleocene Thermal Maximum. *Science*, *286*, 1531–1533.

Kelly, D. C., Bralower, T. J., & Zachos, J. C. (1998). Evolutionary consequences of the latest Paleocene thermal maximum for tropical planktonic foraminifera. *Palaeogeography, Palaeoclimatology, Palaeoecology*, *141*, 139–161.

Kendon, M., McCarthy, M., Jevrejeva, S., Matthews, A., & Legg, T. (2019). State of the UK climate 2018. *International Journal of Climatology*, *39*, 1–55.

Kennett, J. P., Cannariato, K. G., Hendy, I. L., & Behl, R. J. (2000). Carbon isotopic evidence for methane hydrate instability during Quaternary interstadials. *Science*, *288*, 128–133.

Kennett, J. P., Cannariato, K. G., Hendy, I. L., & Behl, R. J. (2003). *Methane hydrates in quaternary climate change: The Clathrate Gun Hypothesis*. Washington, DC: American Geophysical Union.

Kim, J.-H., van der Meer, J., Schouten, S., Helmke, P., Willmott, V., Sangiorgi, F., Koç, N., et al. (2010). New indices and calibrations derived from the distribution of crenarchaeal

isoprenoid tetraether lipids: Implications for past sea surface temperature reconstructions. *Geochimica et Cosmochimica Acta*, *74*, 4639–4654.

Kısakürek, B., Eisenhauer, A., Böhm, F., Garbe-Schönberg, D., & Erez, J. (2008). Controls on shell Mg/Ca and Sr/Ca in cultured planktonic foraminiferan, Globigerinoides ruber (white). *Earth and Planetary Science Letters*, *273*, 260–4654.

Knell, S. J. (2013). *The great fossil enigma: The search for the conodont animal*. Bloomington: Indiana University Press.

Knoll, A. H., Bambach, R. K., Payne, J. L., Pruss, S., & Fischer, W. W. (2007). Paleophysiology and end-Permian mass extinction. *Earth and Planetary Science Letters*, *256*, 295–313.

Krull, E. S., & Retallack, G. J. (2000). $d^{13}C$ depth profiles from paleosols across the Permian-Triassic boundary: Evidence for methane release. *Geological Society of America Bulletin*, *112*, 1459–1472.

Krull, E. S., Retallack, G. J., Campbell, H. J., & Lyon, G. L. (2000). $d^{13}C_{org}$ chemostratigraphy of the Permian-Triassic boundary in the Maitai Group, New Zealand: evidence for high-latitudinal methane release. *New Zealand Journal of Geology and Geophysics*, *43*, 21–32.

Kump, L. R. (2018). Prolonged Late Permian-Early Triassic hyperthermal: Failure of climate regulation? *Philosophical Transactions of the Royal Society A: Mathematical, Physical and Engineering Sciences*, *376*, 20170078.

Kvenvolden, K. A. (1993). Gas hydrates: Geological perspective and global change. *Reviews of Geophysics*, *31*, 173–187.

Labandeira, C. C., & Sepkoski, J. J. Jr. (1993). Insect diversity in the fossil record. *Science*, *261*, 310–315.

Lea, D. W., Pak, D. K., & Spero, H. J. (2000). Climate impact of Late Quaternary Equatorial Pacific sea surface temperature variations. *Science*, *289*, 1719–1724.

Lear, C. H., Bailey, T. R., Pearson, P. N., Coxall, H. K., & Rosenthal, Y. (2008). Cooling and ice growth across the Eocene-Oligocene transition. *Geology*, *36*, 251–254.

Lear, C. H., Elderfield, H., & Wilson, P. A. (2000). Cenozoic deep-sea temperatures and global ice volumes from Mg/Ca in benthic foraminiferal calcite. *Science*, *287*, 269–272.

Li, L., & Keller, G. (1998). Abrupt deep-sea warming at the end of the Cretaceous. *Geology*, *26*, 995–998.

Liu, Z., Pagani, M., Zinniker, D., DeConto, R., Huber, M., Brinkhuis, H., Shah, S. R., Leckie, R. M., et al. (2009). Global cooling during the Eocene-Oligocene climate transition. *Science*, *323*, 1187–1190.

Lunt, D. J., Farnsworth, A., Loptson, C., Foster, G. L., Markwick, P., O'Brien, C. L., Pancost, R. D., et al. (2016). Palaeogeographic controls on climate and proxy interpretation. *Climate of the Past*, *12*, 1181–1198.

Majorowicz, J., Grasby, S. E., Safanda, J., & Beauchamp, B. (2014). Gas hydrate contribution to Late Permian global warming. *Earth and Planetary Science Letters*, *393*, 243–253.

McInerney, F. A., & Wing, S. L. (2011). The Paleocene-Eocene Thermal Maximum: A perturbation of carbon cycle, climate, and biosphere with implications for the future. *Annual Review of Earth and Planetary Sciences*, *39*, 489–516.

Mitsuguchi, T., Matsumoto, E., Abe, O., Uchida, T., & Isdale, P. J. (1996). Mg/Ca thermometry in coral skeletons. *Science*, *274*, 961–963.

Müller, I. A., Fernandez, A., Radke, J., van Dijk, J., Bowen, D., Schwieters, J., & Bernasconi, S. M. (2017). Carbonate clumped isotope analyses with the long-integration dual-inlet (LIDI) workflow: Scratching at the lower sample weight boundaries. *Rapid Communications in Mass Spectrometry*, *31*, 1057–1066

Nürnberg, D., Bijma, J., & Hemleben, C. (1996). Assessing the reliability of magnesium in foraminiferal calcite as a proxy for water mass temperatures. *Geochimica et Cosmochimica Acta*, *60*, 803–814.

O'Connor, M. I., Piehler, M. F., Leech, D. M., Anton, A., & Bruno, J. F. (2009). Warming and resource availability shift food web structure and metabolism. *PLoS Biology*, *7*(8), p.e1000178.

Payne, J. L., & Kump, L. R. (2007). Evidence for recurrent Early Triassic massive volcanism from quantitative interpretation of carbon isotope fluctuations. *Earth and Planetary Science Letters*, *256*, 264–277.

Pearson, P. N., McMillan, I. K., Wade, B. S., Jones, T. D., Coxall, H. K., Bown, P. R., & Lear, C. H. (2008). Extinction and environmental change across the Eocene-Oligocene boundary in Tanzania. *Geology*, *36*, 179–182.

Pearson, P. N., van Dongen, B. E., Nicholas, C. J., Pancost, R. D., Schouten, S., Singano, J. M., & Wade, B. S. (2007). Stable warm tropical climate through the Eocene Epoch. *Geology*, *35*, 211–214.

Penman, D. E. (2016). Silicate weathering and North Atlantic silica burial during the Paleocene-Eocene thermal maximum. *Geology*, *44*, 731–734.

Percival, L. M. E. , Selby, D., Bond, D. P. G., Rakociński, M., Racki, G., Marynowski, L., Adatte, T., et al. (2019). Pulses of enhanced continental weathering associated with multiple Late Devonian climate perturbations: Evidence from osmium-isotope compositions. *Palaeogeography, Palaeoclimatology, Palaeoecology*, *524*, 240–249.

Petchey, O. L., McPhearson, P. T., Casey, T. M., & Morin, P. J. (1999). Environmental warming alters food-web structure and ecosystem function. *Nature*, *402*, 69–72.

Pinto, J. P., Turco, R. P., & Toon, O. B. (1989). Self-limiting physical and chemical effects in volcanic eruption clouds. *Journal of Geophysical Research, 94* (D8), 11165-11.

Pörtner, H. O. (2002). Climate variations and the physiological basis of temperature dependent biogeography: Systemic to molecular hierarchy of thermal tolerance in animals. *Comparative Biochemistry and Physiology Part A: Molecular and Integrative Physiology*, *132*, 739–761.

Pörtner, H. O. (2010). Oxygen-and capacity-limitation of thermal tolerance: A matrix for integrating climate-related stressor effects in marine ecosystems. *Journal of Experimental Biology*, *213*, 881–893.

Pörtner, H. O., & Grieshaber, M. K. (1993). Critical PO_2(s) in oxyconforming and oxyregulating animals gas exchange, metabolic rate and the mode of energy production. In J. E. P. W. Bicudo (Ed.), *The vertebrate gas transport cascade adaptations to environment and mode of life* (pp. 330–357). Boca Raton, FL: CRC Press.

Prahl, F. G., de Lange, G. J., Lyle, M., & Sparrow, M. A. (1989). Post-depositional stability of long-chain alkenones under contrasting redox conditions. *Nature*, *341*, 434–437.

Prahl, F. G., Muehlhausen, L. A., & Zahnle, D. L. (1988). Further evaluation of long-chain alkenones as indicators of paleoceanographic conditions. *Geochimica et Cosmochimica Acta*, *52*, 2303–2310.

Racki, G., & Wignall, P. B. (2005). Late Permian double-phased mass extinction and volcanism: An oceanographic perspective. *Developments in Palaeontology and Stratigraphy*, *20*, 263–297.

Rampino, M. R., Self, S., & Stothers, R. B. (1988). Volcanic winters. *Annual Review of Earth and Planetary Sciences*, *16*, 73–99.

Retallack, G. J. (1995). Permian-Triassic life crisis on land. *Science*, *267*, 77–80.

Retallack, G. J., & Krull, E. S. (2006). Carbon isotopic evidence for terminal-Permian methane outbursts and their role in extinctions of animals, plants coral reefs, and peat swamps. In S. F. Greb, & W. A. Di Michele (Eds.), *Wetlands through time* (pp. 249–268). Geological Society of America Special Paper 399. Boulder, CO: Geological Society of America.

Retallack, G. J., Metzger, C. A., Greaver, T., Jahren, A. H., Smith, R. M. H., & Sheldon, N. D. (2006). Middle-Late Permian mass extinction on land. *Geological Society of America Bulletin*, *118*, 1398–1411.

Robinson, S. A., Ruhl, M., Astley, D. L., Naafs, B. D. A., Farnsworth, A. J., Bown, P. R., Jenkyns, H. C., et al. (2017). Early Jurassic North Atlantic sea surface temperatures from TEX 86 palaeothermometry. *Sedimentology*, *64*, 215–230.

Robock, A. (2000). Volcanic eruptions and climate. *Reviews of Geophysics*, *38*, 191–219.

Ruhl, M., Bonis, N. R., Reichart, G. J., Damsté, J. S. S., & Kürschner, W. M. (2011). Atmospheric carbon injection linked to end-Triassic mass extinction. *Science*, *333*, 430–434.

Rupple, C. D. (2011). Methane hydrates and contemporary climate change. *Nature Education Knowledge*, *2*, 12.

Russell, B. D., Connell, S. D., Findlay, H. S., Tait, K., Widdicombe, S., & Mieszkowska, N. (2013). Ocean acidification and rising temperatures may increase biofilm primary productivity but decrease grazer consumption. *Philosophical Transactions of the Royal Society Series B*, *368* (1627), 20120438.

Scarth, A. (2001). *Vulcan's fury: Man against the volcano*. New Haven: Yale University Press.

Scheibner, C., & Speijer, R. P. (2008). Late Paleocene–early Eocene Tethyan carbonate platform evolution: A response to long-and short-term paleoclimatic change. *Earth Science Reviews*, *90*, 71–102.

Schmidt, A., Carslaw, K. S., Mann, G. W., Rap, A., Pringle, K. J., Spracklen, D. V., et al. (2012). Importance of tropospheric volcanic aerosol for indirect radiative forcing of climate. *Atmospheric Chemistry and Physics*, *12*(16), 7321–7339.

Schmidt, A., Skeffington, R. A., Thordarson, T., Self, S., Forster, P. M., Rap, A., et al. (2016). Selective environmental stress from sulphur emitted by continental flood basalt eruptions. *Nature Geoscience*, *9*(1), 77–82.

Schmidt, G. A., Bigg, G. R., & Rohling, E. J., (1999). Global seawater oxygen-18 database: *v1*.21. http://data.giss.nassa.gov/o18data/

Schouten, S., Hopmans, E. C., Schefuß, E., & Sinninghe Damsté, J. S. (2002). Distributional variations in marine crenarchaeotal membrane lipids: a new tool for reconstructing ancient sea water temperatures? *Earth and Planetary Science Letters*, *204*, 265–274.

Scripps (2018). *The Keeling curve*. https://scripps.ucsd.edu/programs/keelingcurve/pdf-downloads/

Sear, C. B., Kelly, P. M., Jones, P. D., & Goodess, C. M. (1987). Global surface-temperature responses to major volcanic eruptions. *Nature*, *330*, 365.

Self, S., Thordarson, T., & Widdowson, M. (2005). Gas fluxes from flood basalt eruptions. *Elements*, *1*, 283–287.

Sephton, M. A., Jiao, D., Engel, M. H., Looy, C. V., & Visscher, H. (2015). Terrestrial acidification during the end-Permian biosphere crisis? *Geology*, *43*, 159–162.

Sharp, Z. (2017). *Principles of stable isotope geochemistry, 2nd ed. University of New Mexico.* doi: 10.5072/FK2GB24S9F

Smith, R. M., & Ward, P. D. (2001). Pattern of vertebrate extinctions across an event bed at the Permian-Triassic boundary in the Karoo Basin of South Africa. *Geology*, *29*, 1147–1150.

Sobolev, S. V., Sobolev, A. V., Kuzmin, D. V., Krivolutskaya, N. A., Petrunin, A. G., Arndt, N. T., et al. (2011). Linking mantle plumes, large igneous provinces and environmental catastrophes. *Nature*, *477*, 312–316.

Song, H.-J., Wignall, P. B., Chu, D. -L., Tong, J., Sun, Y.-D., Song, H.-Y., et al. (2014). Anoxia/high temperature double whammy during the Permian-Triassic marine crisis and its aftermath. *Scientific Reports*, *4*, 4132. doi: 10.1038/srep04132.

Stauffer, B. A., Gellene, A. G., Schnetzer, A., Seubert, E. L., Oberg, C., Sukhatme, G. S., & Caron, D. A. (2012). An oceanographic, meteorological, and biological 'perfect storm' yields a massive fish kill. *Marine Ecology Progress Series*, *468*, 231–243.

Sun, Y.-D., Joachimski, M. M., Wignall, P. B., Yan, C.-B., Chen, Y.-L., Jiang, H.-S., et al. (2012). Lethally hot temperatures during the Early Triassic greenhouse. *Science*, *338*, 366–370.

Sun, Y.-D., Zulla, M. J., Joachimski, M. M., Bond, D. P. G., Wignall, P. B., Zhang, Z. T., & Zhang, M. H. (2019). Ammonium ocean following the end-Permian mass extinction. *Earth and Planetary Science Letters*, *518*, 211–222.

Svensen, H., Planke, S., Malthe-Sørenssen, A., Jamtveit, B., Myklebust, R., Eidem, T. R., & Rey, S. S. (2004). Release of methane from a volcanic basin as a mechanism for initial Eocene global warming. *Nature*, *429*, 542–545.

Svensen, H., Planke, S., Polozov, A. G., Schmidbauer, N., Corfu, F., Podladchikov, Y. Y., & Jamtveit, B. (2009). Siberian gas venting and the end-Permian environmental crisis. *Earth and Planetary Science Letters*, *277*, 490–500.

Thomas, E. (1998). Biogeography of the late Paleocene benthic foraminiferal extinction. In M.-P. Aubry, S. G. Lucas, & W. A. Berggren (Eds.), *Late Paleocene-Early Eocene climatic and biotic events in the marine and terrestrial records* (pp. 214–243). New York: Columbia University Press.

Thomas, E., & Shackleton, N. J. (1996). The Paleocene-Eocene benthic foraminiferal extinction and sTable isotope anomalies. *Geological Society of London Special Publications*, *101*, 401–441.

Thordarson, T., & Self, S. (1993). The Laki (Skaftár Fires) and Grímsvötn eruptions in 1783–1785. *Bulletin of Volcanology*, *55*, 233–263.

Thordarson, T., & Self, S. (2003). Atmospheric and environmental effects of the 1783–1784 Laki eruption: A review and reassessment. *Journal of Geophysical Research: Atmospheres*, *108* (D1), AAC 7-1–AAC 7-29.

Tripati, A. K., Delaney, M. L., Zachos, J. C., Anderson, L. D., Kelly, D. C., & Elderfield, H. (2003). Tropical sea-surface temperature reconstruction for the early Paleogene using Mg/Ca ratios of planktonic foraminifera. *Paleoceanography*, *18*(4).

Tu, C., Chen, Z. Q., & Harper, D. A. (2016). Permian-Triassic evolution of the bivalvia: Extinction-recovery patterns linked to ecologic and taxonomic selectivity. *Palaeogeography, Palaeoclimatology, Palaeoecology*, *459*, 53–62.

Turner, S. K. (2018). Constraints on the onset duration of the Paleocene-Eocene Thermal Maximum. *Philosophical Transactions of the Royal Society A: Mathematical, Physical and Engineering Sciences*, *376*, 20170082.

Veizer, J., & Prokoph, A. (2015). Temperatures and oxygen isotopic composition of Phanerozoic oceans. *Earth-Science Reviews*, *146*, 92–104.

Veizer, J., Ala, D., Azmy, K., Bruckschen, P., Buhl, D., Bruhn, F., et al. (1999). $^{87}Sr/^{86}Sr$, $\delta^{13}C$ and $\delta^{18}O$ evolution of Phanerozoic seawater. *Chemical Geology*, *161*(1–3), 59–88.

Weijers, J. W. H., Schouten, S., Spaargaren, O. C., & Sinninghe Damsté, J. S. (2006). Occurrence and distribution of tetraether membrane lipids in soils: Implications for the use of the TEX_{86} proxy and the BIT index. *Organic Geochemistry*, *37*, 1680–1693

Wignall, P. B. (2007). The end-Permian mass extinction: How bad did it get? *Geobiology*, *5*, 303–309.

Wignall, P. B. (2015). *The worst of times: How Life on Earth survived eighty million years of extinctions*. Princeton: Princeton University Press.

Wilf, P., Johnson, K. R., & Huber, B. T. (2003). Correlated terrestrial and marine evidence for global climate changes before mass extinction at the Cretaceous-Paleogene boundary. *Proceedings of the National Academy of Sciences of the United States of America*, *100*, 599–604.

Wood, C. A. (1992). Climatic effects of the 1783 Laki eruption. In C. R. Harrington (Ed.), *The year without a summer: World climate in 1816* (pp. 58–77). Ottawa, Canada: Canadian Museum of Nature.

Zachos, J. C., Röhl, U., Schellenberg, S. A., Sluijs, A., Hodell, D. A., Kelly, D. C., et al. (2005). Rapid acidification of the ocean during the Paleocene-Eocene thermal maximum. *Science*, *308*, 1611–1615.

Zachos, J. C., Schouten, S., Bohaty, S., Quattlebaum, T., Sluijs, A., Brinkhuis, H., Gibbs, S. J., et al. (2006). Extreme warming of mid-latitude coastal ocean during the Paleocene-Eocene Thermal Maximum: Inferences from TEX_{86} and isotope data. *Geology*, *34*, 737–740.

Zaffos, A., Finnegan, S., & Peters, S. E. (2017). Plate tectonic regulation of global marine animal diversity. *Proceedings of the National Academy of Sciences*, 201702297.

Zeebe, R. E., Dickens, G. R., Ridgwell, A., Sluijs, A., & Thomas, E. (2014). Onset of carbon isotope excursion at the Paleocene-Eocene thermal maximum took millennia, not 13 years. *Proceedings of the National Academy of Sciences*, *111*, E1062–E1063.

Zeebe, R. E., Zachos, J. C., & Dickens, G. R. (2009). Carbon dioxide forcing alone insufficient to explain Palaeocene-Eocene Thermal Maximum warming. *Nature Geoscience*, *2*, 576–580.

Zhao, M., & Running, S. W. (2010). Drought-induced reduction in global terrestrial net primary production from 2000 through 2009. *Science*, *329*, 940–943.

Zheng, Y., Heng, P., Conte, M. H., Vachula, R. S., & Huang, Y. (2019). Systematic chemotaxonomic profiling and novel paleotemperature indices based on alkenones and alkenoates: Potential for disentangling mixed species input. *Organic Geochemistry*, *128*, 26–41.